JOC The Journal of Organic Chemistry

pubs.acs.org/joc Article

Design and Synthesis of RhodIndolizine Dyes with Improved Stability and Shortwave Infrared Emission up to 1250 nm

Satadru Chatterjee, Abdul Kalam Shaik, Kalpani Hirunika Wijesinghe, David Ndaleh, Amala Dass, Nathan I. Hammer,* and Jared H. Delcamp*

Cite This: *J. Org. Chem.* 2022, 87, 11319−11328 Read Online

ACCESS | Metrics & More | Article Recommendations | Supporting Information

ABSTRACT: The design of shortwave infrared (SWIR) emissive small molecules with good stability in water remains an important challenge for fluorescence biological imaging applications. A series of four SWIR emissive rhodindolizine (RI) dyes were rationally designed and synthesized to probe the effects of nonconjugated substituents, conjugated donor groups, and nanoencapsulation in a water-soluble polymer on the stability and optical properties of the dyes. Steric protecting groups were added at the site of a significant LUMO presence to probe the effects on stability. Indolizine donor groups with added dimethylaniline groups were added to reduce the electrophilicity of the dyes toward nucleophiles such as water. All of the dyes were found to absorb (920−1096 nm peak values) and emit (1082−1256 nm peak values) within the SWIR region. Among xanthene-based emissive dyes, emission values >1200 nm are exceptional with 1256 nm peak emission being a longer emission than the recent record setting VIX-4 xanthene-based dye. Half-lives were improved from ∼5 to >24 h through the incorporation of either steric-based core protection groups or donors with increased donation strength. Importantly, the nanoencapsulation of the dyes in a water-soluble surfactant (Triton-X) allows for the use of these dyes in biological imaging applications.

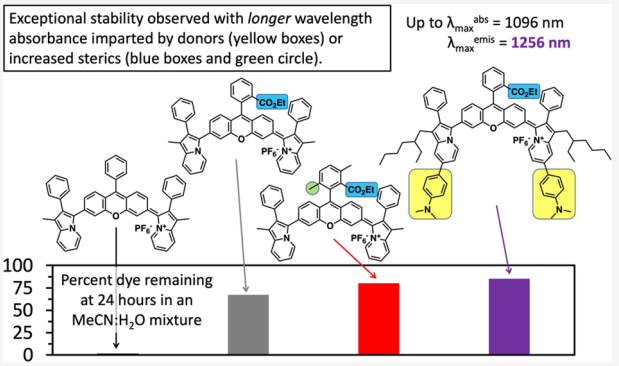

INTRODUCTION

Recent *in vivo* fluorescent imaging examples in the shortwave infrared (SWIR, 1000−3000 nm) spectral region have provided some of the highest-resolution and highest-frame-rate images known.[1−7] Interestingly, image quality has continued to be improved as longer wavelengths are accessed through dye designs with water serving to enhance the contrast in this spectral region by limiting background noise (i.e., tissue fluorescence and scattered light).[8,9] Thus, longer-wavelength-absorbing and -emitting dyes are needed to further improve *in vivo* fluorescence imaging. Importantly, many near-infrared (NIR) and SWIR materials rely on cationic conjugated π-systems for longer-wavelength access. These cationic systems (e.g., squaraines, cyanines, and xanthenes) are often susceptible to nucleophilic addition even from weak nucleophiles such as water.[10−14] Thus, two key parameters with respect to the dye are needed to improve *in vivo* SWIR imaging: shorter wavelength accessing dyes and dyes with increased stability.

Rhodamines, which are xanthene-based, are widely used as fluorescent probes due to their high absorption coefficients and high fluorescence quantum yields.[15] However, these dyes typically absorb and emit in the visible spectral region (∼550 nm), which limits *in vivo* applications due to tissue absorbance and autofluorescence in this region.[8,16−18] An intriguing research direction focuses on shifting these strongly absorbing and brightly emitting compounds toward using longer wavelengths. One of the most common strategies is to exchange the oxygen atom on the xanthene core for numerous other elements now known to shift the absorption and emission toward accessing longer wavelengths.[19−24] A second approach focuses on exchanging the nitrogen groups on rhodamine with π-conjugated carbon-based groups which has recently been shown to give some of the longest wavelength absorbing and -emitting xanthene-based materials known.[1,25,26]

Rhodindolizine (RI) is similar to rhodamine with the amine groups replaced with indolizine heterocycle groups (Figure 1).[25] Rhodindolizine gave one of the longest-wavelength-emitting xanthene-based materials known at the time at 1092 nm. Only recently have longer-wavelength-emitting xanthene-based systems been identified as VIX-4 with peak emission at 1210 nm in dichloromethane.[1] VIX-4 makes use of two julolidinestyryl groups on the xanthene core used to better delocalize the xanthene cation. The approach to better cation

Received: March 24, 2022
Published: August 19, 2022

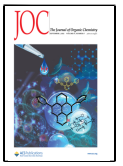

https://doi.org/10.1021/acs.joc.2c00678
J. Org. Chem. 2022, 87, 11319−11328

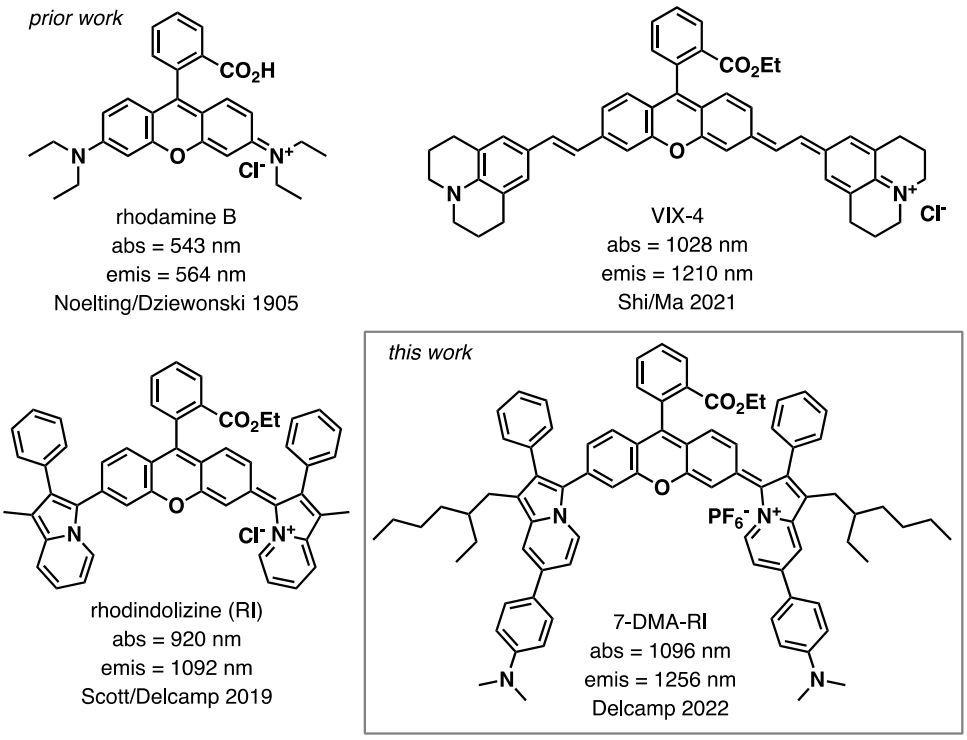

Figure 1. Comparison of absorption and emission wavelengths of rhodamine B, rhodindolizine (RI), VIX-4, and 7-DMA-RI (this work).

delocalization is intriguing, thus the design of a rhodindolizine dye with added *N,N*-dimethylaniline (DMA) donors on the indolizine periphery was pursued (coded 7-DMA-RI, Figures 1 and 2). We reasoned that due to the fully conjugated nature of indolizine, these added donors could serve to shift the absorption and emission of rhodindolizine further toward longer wavelengths by delocalizing the cation on xanthene. We reasoned a secondary effect of this dye design would be on improving dye stability by reducing the electrophilicity of the dye cation as has been shown with rhodamine-based dyes.[24] Additionally, we sought to probe the effects on dye stability through sterically blocking the xanthene core, modulating electronics at the aryl ring on the xanthene core, and nanoencapsulating the dye. To evaluate these approaches, a series of rhodindolizine dyes were designed, synthesized, and characterized with comparison to recently reported rosindolizine dyes (Figure 1).[11]

RI, ^{tol}RosIndz, and ^{Ph}RosIndz have been previously reported and serve as benchmarking materials in the stability studies (Figure 2).[11,25] Sterics at the central core of xanthene-based materials have been reported to be important for material stability.[22] To probe the importance of this design element within the RI framework, dimethyl-substituted dye Me2-RI was targeted. Multiple literature reports suggest that the electron density at the aryl ring on the xanthene core may be important to the stability of fluorescent rhodamine dyes.[27,28] To probe this possibility within the RI framework, dyes AMD-RI (more electron-rich carbonyl) and CF3-RI (less electron-rich carbonyl) were targeted for comparison to the parent RI structure. As mentioned above, the 7-DMA-RI dye was targeted to prove the effect of increased donor strength on dye stability and spectral region shifts in absorption and emission. C4CC-RI was targeted to illustrate the ease of bioconjugatable group installation within this design. The absorption and emission properties of the dyes were measured in varied solvent environments along with half-life data in the presence of acetonitrile with added water to probe stability and the effects of derivatizations on the dye's optical properties.

RESULTS AND DISCUSSION

Benchmark materials RI, ^{tol}RosIndz, and ^{Ph}RosIndz have been previously reported.[11,25] However, since the original report of ^{Ph}RosIndz, a crystal structure of the material was obtained via a crystal obtained by diffusion of diethyl ether into an acetonitrile solution of the compound, which is reported herein for the first time (Figure 3). The crystal structure reveals that the phenyl group is perpendicular to the xanthene core on this dye. Thus, substituents ortho to the xanthene group on the phenyl ring would extend over the xanthene π-face and could be used to sterically block the xanthene core from nucleophilic attack. The xanthene core was found to have a significant accumulation of the lowest unoccupied molecular orbital (LUMO) at the central carbon of the xanthene core where the phenyl group attaches via density functional theory (DFT) computational analysis at the B3LYP/6-311G(d,p) level of theory with dichloromethane as an implicit solvent via a polarized continuum model[29−31] and the Gaussian16 software package (Figure 3).[32−35] Indeed, this observation is in agreement with the reported substantially improved stability of ^{tol}RosIndz relative to ^{Ph}RosIndz since the LUMO would be expected to be the sight of addition of a nucleophile such as water.[11] Thus, the methyl group of the Me2-RI derivative would be expected to have a large influence on dye stability with the larger methyl group blocking the LUMO at the central xanthene carbon compared to the hydrogen of RI (Figure 3).

The synthesis of AMD-RI and C4CC-RI begins from known lactone **1** (Scheme 1).[25] The yellow-orange lactone **1** is opened upon being heated in a dichloroethane solution of $POCl_3$ to presumably give the deep green acid chloride **2** (Scheme 1). Crude **2** can then either be exposed to

https://doi.org/10.1021/acs.joc.2c00678
J. Org. Chem. 2022, 87, 11319−11328

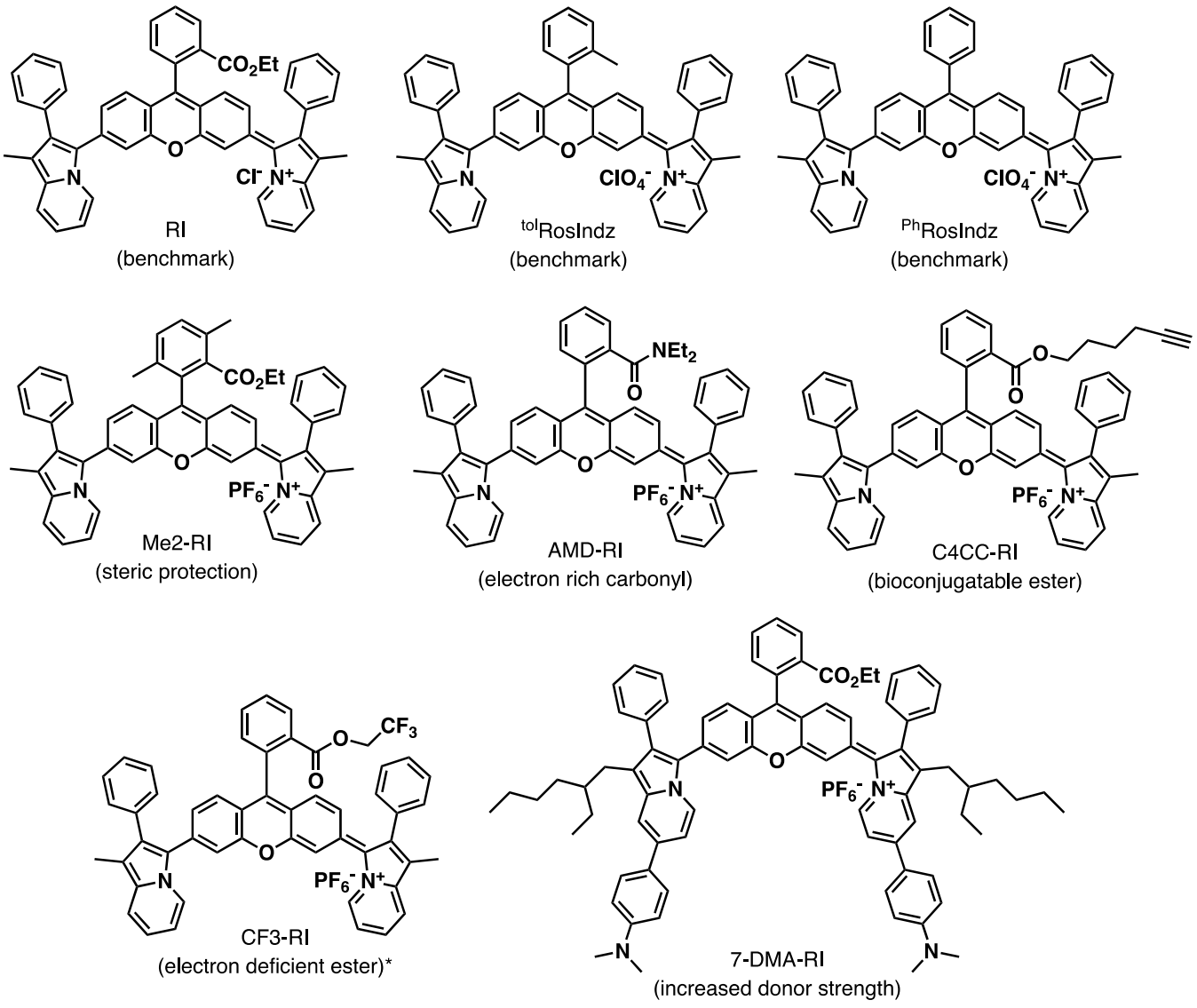

Figure 2. Target and benchmark comparison dyes in this study with comparative properties listed. * Indicates that the dye could not be successfully characterized due to rapid decomposition but could be observed via optical spectroscopy.

diethylamine (DEA) or 5-hexyn-1-ol to give AMD-RI (61% yield) and C4CC-RI (59% yield), respectively, as the PF_6^- salts after anion exchange. The anions were exchanged to allow for easier purification. Me2-RI was synthesized beginning from known 3,6-dimethylphthalic anhydride (**3**)[36] and commercial 3-bromophenol (**4**) via heating for 3 days in triflic acid in a sealed tube to give lactone **5**. Milder reactions more commonly associated with the formation of lactones such as **8** were not successful presumably due to significant steric congestion at the spiro lactone carbon center.[37] Lactone **5** underwent palladium-catalyzed double C−H activation with indolizine **6** to give lactone **7** in a 48% yield. Exposure to $POCl_3$ followed by EtOH led to Me2-RI in a 59% yield after anion exchange. 7-DMA-RI was synthesized beginning from known lactone **8**[37] and known indolizine **9**[38] via palladium-catalyzed C−H activation to give lactone **10**. Lactone opening via $POCl_3$ and exposure to EtOH led to the formation of 7-DMA-RI after anion exchange. In general, the synthetic pathways to these dyes were concise with the largest number of steps being 6 from commercial materials to form 7-DMA-RI.

The target and benchmark materials were analyzed by absorption and emission spectroscopy next (Figure 4, Table 1). The absorption and emission curve shapes were similar for RI, Me2-RI, C4CC-RI, and AMD-RI with only slight changes in the absorption maxima (λ_{max}^{abs}) and molar absorptivity (ε) values in toluene (926−943 nm and 70,000−98,000 $M^{-1}cm^{-1}$, respectively). The close values observed from the absorption spectroscopy measurements are expected for these materials since substitutions are all on the benzene group that is out of plane with the xanthene core. However, the 7-DMA-RI derivative shows a substantial shift in the λ_{max}^{abs} value relative to the remaining derivatives by at least 153 nm to give a λ_{max}^{abs} of 1096 nm. The ε value of the 7-DMA-RI derivative is observed to be 71,000 $M^{-1}cm^{-1}$. This shift in absorption wavelength to lower values suggests significant involvement of the DMA groups with respect to the HOMO since these groups are π-electron rich. Indeed, DFT studies reveal that the highest occupied molecular orbital (HOMO) delocalizes from the xanthene core onto the indolizine rings and the DMA groups with a similar shift of vertical transition energies observed via time-dependent (TD)-DFT as is observed

https://doi.org/10.1021/acs.joc.2c00678
J. Org. Chem. 2022, 87, 11319−11328

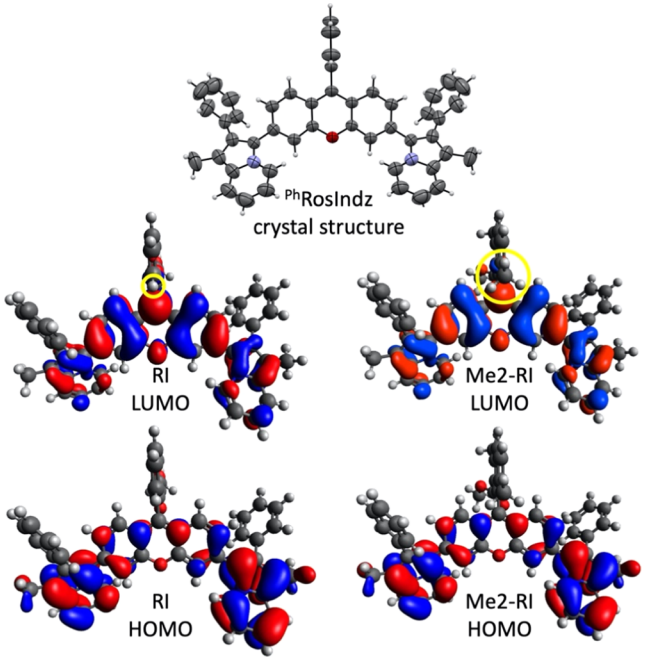

Figure 3. Crystal structure of ^{Ph}RosIndz with $[ClO_4]^-$ removed for clarity and ellipsoids drawn at 50% probability. HOMO and LUMO orbitals of RI and Me2-RI. The yellow circles indicate the size of the group blocking the LUMO orbital at the center of the xanthene core.

experimentally via absorption spectroscopy when 7-DMA-RI and RI are compared (Figure 5 and Table S2). Thus, the 7-DMA-indolizine donor group can be considered a π-extended, more electron-rich version of the parent indolizine heterocycle with strong electronic communication across the indolizine from the DMA group.

The absorption onset values (~1100−1300 nm) of all of the compounds are well within the SWIR domain with the 7-DMA-RI dye having the λ_{max}^{abs} value within the SWIR region as well. All of the RI dyes were found to emit in the SWIR region with peak emission (λ_{max}^{em}) values with RI, C4CC-RI, Me2-RI, and AMD-RI λ_{max}^{em} values ranging from 1085 to 1096 nm with emission onset values tailing to ≥1400 nm. The λ_{max}^{em} value observed with 7-DMA-RI is at 1256 nm with emission onset >1400 nm. The relative quantum yield values were obtained using IR-1061 with a reference quantum yield value of 0.32 ± 0.04% as reported by Sletten and co-workers when IR26 is taken to have a quantum yield value of 0.05 ± 0.03% (Table 1).[39] We note that a range of quantum yield reference values are reported for IR-1061 with some careful assessments suggesting a value of 0.59%.[40] Relative quantum yield values taking IR-1061 as 0.59% are reported in the supporting information (Table S1). The 0.32% quantum yield value for IR-1061 is used in the main text since our labs have obtained a similar value for IR-1061 (0.28%, which is within the reported error) when measuring relative to IR26 taken at 0.05% as is commonly done in the literature.[4,41] Within the series of dyes absorbing and emitting at similar wavelengths (RI, C4CC-RI, Me2-RI, and AMD-RI), the quantum yield values vary by approximately a factor of 2 from 0.005 to 0.010% with the Me2-RI dye being appreciably higher than the other two derivatives. 7-DMA-RI has a quantum yield of 0.005%, which is expected to be lower when comparing similar core materials due to the energy gap law.[42] The molecular brightness (MB) was found via the equation MB = $\varepsilon \times \phi$ for the RI dyes with values ranging from 4 to 9 in the SWIR region. Importantly, MB values near this range have demonstrated good image quality via *in vivo* studies.[3]

Stability studies of the RI dyes were conducted in an acetonitrile (ACN): water mixture (99:1) to examine the effects of derivatization on the rate of dye decomposition in the presence of water and ambient light (Figure 6). These conditions were selected since the RI dyes have almost no appreciable decomposition issues in anhydrous solvents such as acetonitrile, toluene, or dichloromethane; however, polar protic solvents such as methanol and ethanol were found to lead to loss of dye absorptivity over time. Water was selected as a quantification solvent of this effect due to the practical relevance of water with respect to biological imaging. Both RI dyes and RosIndz dyes were probed in these studies by making solutions of the dyes and monitoring the λ_{max}^{abs} values over time with the samples kept under ambient conditions with ambient fluorescent lighting present. The ratio of the λ_{max}^{abs} values at time zero (abs_0) to the values over time was tracked and is plotted in Figure 6. Several design element trends were evident from these studies. The fastest decomposing dye was ^{Ph}RosIndz (half-life of ~7 h), which has no sterically blocking groups at the benzene ring attached to the xanthene core. Introduction of an ethyl ester group (RI), hex-1-ynyl ester (C4CC-RI), or a methyl group (^{tol}RosIndz) to the benzene ring on the xanthene core led to an improved stability with half-lives of >24, 17, and 11 h observed. This suggests that sterically blocking a face of the xanthene core has substantial effects on the dye stability in aqueous environments. Replacing the ethyl ester group with a *N*,*N*-diethylamide group as a more electron-rich carbonyl led to an increase in the dye decomposition rate matching that of the unsubstituted ^{Ph}RosIndz with a half-life of ~7 h. It is not clear if this effect is due to stronger hydrogen bonding of the amide pre-coordinating nucleophilic water or if the more electron-rich carbonyl is leading to more rapid decomposition. To probe this, CF3-RI was synthesized; however, the compound was found to decompose on the second to minute timescale during isolation, suggesting that electron-deficient carbonyls are exceptionally sensitive on these dyes. Addition of a methyl group on the benzene ring ortho to the xanthene core (Me2-RI relative RI) led to another dramatic improvement in stability in the presence of water with 80% of the absorbance remaining for Me2-RI after 24 h (versus 67% for RI). Thus, protecting both faces of the xanthene core sterically leads to a dramatic improvement of the dye stability. To probe the effects of added electron density on dye stability, 7-DMA-RI is compared to RI, which varies by the addition of electron-rich *N*,*N*-dimethylaniline groups to the indolizine periphery. This leads to a dramatic improvement in stability in an aqueous environment with 85% of the initial absorbance of 7-DMA-RI remaining after 24 h (versus 67% with RI). This result suggests that increasing the peripheral donor strength leads to an improved stability toward nucleophilic water.

Encapsulation in water-soluble nanoparticles was undertaken with Triton X100 as a polymer encapsulation agent commonly used in the literature.[43] In this system, RI retains emissive properties in aqueous solution with a near-identical absorption and emission spectrum to that observed in toluene (Figure 4). The nanoencapsulated RI in pure water was found to initially decompose at a similar rate to the RI in a 1:1 acetonitrile/water mixture, which indicates that the nanoparticle is providing no significant enhancement in dye stabilization to

https://doi.org/10.1021/acs.joc.2c00678
J. Org. Chem. 2022, 87, 11319−11328

Scheme 1. Synthesis of a New Class of RhodIndz Molecules

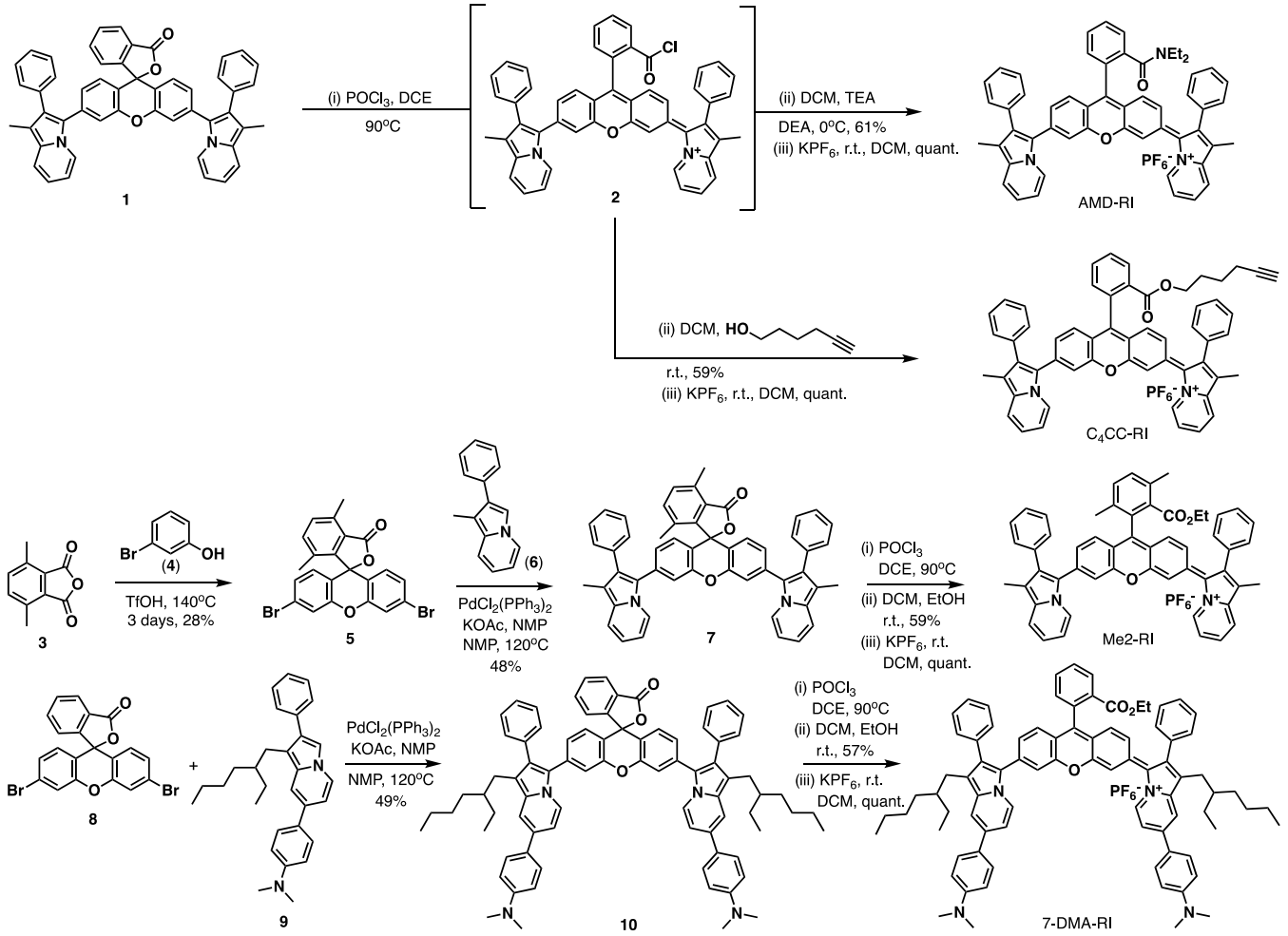

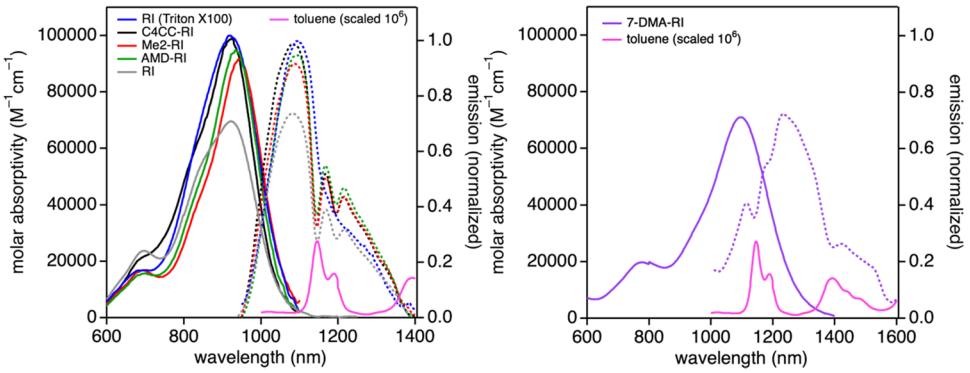

Figure 4. Left: Absorbance (solid lines) and emission (dashed lines, excitation at 919 nm) spectra of C4CC-RI, Me2-RI, RI, and AMD-RI in toluene (25 μM) and RI (nanoencapsulated in Triton X100) in water. Right: Absorption (solid lines) and emission (dashed lines, excitation at 992 nm) spectra of 7-DMA-RI in toluene (25 μM). Note: the local minimum features in the 1100−1250 nm region of the dye emission spectrum are due to solvent absorption of the dye emission. The absorbance spectrum of toluene (pink curve) has the molar absorptivity scaled by 10^6 to account for the concentration of toluene being roughly 10^6 higher than that of the dye.

water (Figure S17). Under these conditions, ∼50% of RI remains at 2 h, which provides an opportunity to formulate and directly use these dyes in an *in vivo* environment for biological imaging.

■ CONCLUSIONS

Four novel rhodindolizine dyes were prepared with varied steric elements at the xanthene core, electronics at the indolizine donors, and functionality for click reactions on the dyes. These dyes were characterized photophysically via steady-state absorption and emission spectroscopy to show appreciable SWIR absorption (λ_{max}^{abs} = 926−1096 nm with onsets all >1000 nm) and emission (λ_{max}^{em} = 1082−1256 nm). The most electron-rich indolizine group leads to peak absorption and emission in the SWIR region (1096 and 1256 nm, respectively) to yield the shortest-wavelength single

https://doi.org/10.1021/acs.joc.2c00678
J. Org. Chem. 2022, 87, 11319−11328

Table 1. Photophysical Characterization of the Synthesized Rhodindolizine Dyes[a]

dye	λ_{max}^{abs} (nm)	λ_{max}^{em} (nm)	ε (M^{-1} cm^{-1})	SS (nmleV)	ϕ (%)	MB ($\varepsilon \times \phi$)
C4CC-RI	926	1085	97,000	159|0.19	0.007	7
Me2-RI	943	1088	90,000	143|0.18	0.005	5
AMD-RI	934	1096	93,000	162|0.19	0.010	9
7-DMA-RI	1096	1256	71,000	160|0.15	0.005	4
RI[b]	926	1082	70,000	156|0.19	0.005	4
RI (Triton X100)[c]	920	1094		174|0.21	0.001	

[a]All values are reported in toluene (25 μM) unless otherwise noted. Quantum yields were calculated by taking the average from three trials. [b]Limited solubility in toluene is observed, which required overnight stirring to dissolve RI with potential slight aggregation as a shoulder appearing in the absorption spectrum relative to dichloromethane (Figure S16). A prior report has a ϕ value of 0.03% in dichloromethane.[25] [c]Indicates the data is collected in H_2O.

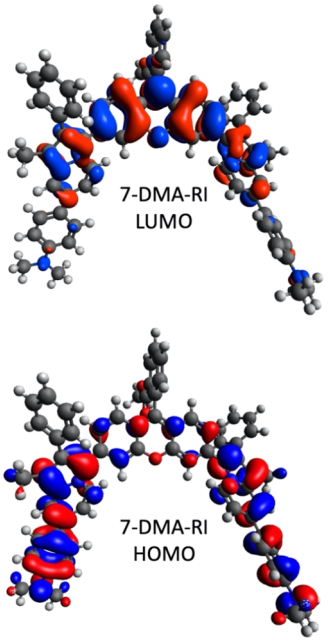

Figure 5. HOMO (bottom) and LUMO (top) orbitals of 7-DMA-RI.

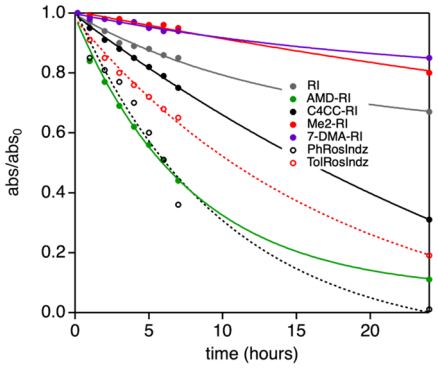

Figure 6. Stability studies of dyes in ACN/H_2O (99:1) under ambient light conditions.

xanthene core-based small molecule (7-DMA-RI) to the best of our knowledge which surpasses the emission maxima of VIX-4 by 46 nm further into the SWIR region. The dyes were analyzed via stability studies in an aqueous environment under ambient atmosphere and lighting. Clear treads of increased sterics near the xanthene core and increased electron density at the donor group positions lead to dramatic improvements in dye stability. These results provide new longer-wavelength-emitting xanthene-based materials for *in vivo* applications as well as show xanthene dye design elements that are needed for improved stability. Future studies are focused on further shifting the absorption and emission wavelengths toward shorter wavelengths using the dye design properties observed here.

EXPERIMENTAL SECTION

General Information. All of the reagents and solvents used in this study were purchased from Sigma-Aldrich, Acros Organics, and Thermo Fischer Scientific. Benchmark materials RI, ^{tol}RosIndz, and ^{Ph}RosIndz have been previously reported.[11,25] Compounds **1**,[25] **3**,[36] **6**,[38] **8**,[37] and **9**[38] have been previously reported. All reactions were heated in oil baths. All of the ^{1}H and ^{13}C NMR spectra were recorded on a Bruker 400 MHz spectrometer using deuterated solvents. *J* values are given in Hz, and chemical shifts are reported in ppm using a residual protiated solvent as a reference. Singlet (s), doublet (d), double doublet (dd), triplet (t), and multiplet (m) were designated as ^{1}H NMR multiplicity patterns. Silica gel (230−400 mesh) and cyano functionalize silica gel columns (RediSep, "Cyano Column" by Isco, if noted in the preparation details below) were used for chromatographic separations either via flash chromatography or with a CombiFlash Rf+ system. A Waters Synapt XS mass spectrometer with a quadrupole time of flight (TOF) was used to collect all electrospray ionization (ESI) mass spectrometry data. Infrared spectra were recorded with an Agilent Cary 660 attenuated total reflection-Fourier transform infrared (ATR-FT-IR) spectrometer. Fluorescence spectra were acquired using a Horiba QuantaMaster 8075-21 spectrofluorometer with xenon lamp excitation and a liquid nitrogen cooled InGaAs solid state detector. The absorption spectra were recorded on a Cary 5000 UV−vis−NIR spectrophotometer. X-ray crystallography was performed in a Rigaku XtaLAB Synergy, Dualflex, HyPix diffractometer.

Synthetic Procedures. *(Z)-3-(9-(2-(Diethylcarbamoyl)phenyl)-6-(1-methyl-2-phenylindolizin-3-yl)-3H-xanthen-3-ylidene)-1-methyl-2-phenyl-3H-indolizin-4-ium hexafluorophosphate (AMD-RI).* To a flame-dried round-bottom flask were added 3′,6′-bis(1-methyl-2-phenylindolizin-3-yl)-3*H*-spiro[isobenzofuran-1,9′-xanthen]-3-one (compound **1**, 50 mg, 0.07 mmol), dry dichloroethane (2 mL, 0.035 M), and $POCl_3$ (33 μL, 0.35 mmol) dropwise. This solution was degassed with N_2 for 10 min and then refluxed overnight under a N_2 atmosphere. Then, the volatiles were removed via a rotary evaporator. The mixture was diluted with dry dichloromethane (2 mL), degassed with N_2 for 5 min, and then, diethylamine (10 μL, 0.08 mmol) and triethylamine (20 μL, 0.14 mmol) were added. The mixture was then stirred at room temperature and monitored via absorption spectroscopy. After the product peak ceased to increase in intensity, the volatiles were evaporated and the crude material was stirred in dichloromethane (~2 mL) over excess solid KPF_6 (~50 mg) under a nitrogen atmosphere overnight. The solids and the liquids were then separated, the volatiles were evaporated, and the compound was directly subjected to column chromatography using a cyano-functionalized silica column with 10% acetonitrile/90% dichloromethane as the eluent to give the desired dye as a green solid (61%, 32 mg, 0.04 mmol). ^{1}H NMR (400 MHz, CD_3CN) δ 8.62

https://doi.org/10.1021/acs.joc.2c00678
J. Org. Chem. 2022, 87, 11319−11328

(d, J = 7.1 Hz, 2H), 7.76−7.70 (m, 3H), 7.60 (d, J = 7.8 Hz, 2H), 7.53 (s, 2H), 7.47−7.34 (m, 9H), 7.26−7.22 (m, 6H), 7.12 (t, J = 6.6 Hz, 2H), 6.83 (t, J = 6.3 Hz, 2H), 3.28−3.17 (m, 4H), 2.23 (s, 6H), 1.15 (t, J = 7.1 Hz, 3H), 0.61 (t, J = 7 Hz, 3H). $^{13}C\{^1H\}$ NMR (100 MHz, CD_3CN) δ 168.2, 156.2, 142.3, 136.9, 135.0, 134.1, 131.3, 131.0, 130.5, 129.9, 129.3, 128.4, 128.1, 127.5, 124.6, 123.3, 122.3, 121.6, 118.8, 114.4, 114.3, 113.8, 44.3, 40.2, 13.6, 11.6, 8.9. Note: Four aromatic carbon signals in the ^{13}C spectrum may have identical shifts to reported signals due to significant congestion with 25 expected aromatic signals. Several signals indeed appear significantly larger than other signals in the ^{13}C spectrum. Overlap with the CD_3CN signal is also possible. ^{19}F NMR (376 MHz, CD_3CN) δ −72.96 (d, J = 705 Hz). ^{31}P NMR (162 MHz, CD_3CN) δ −144.63 (septet, J = 705 Hz). FT-IR (neat, cm^{-1}): 3640, 3533, 3160, 2955, 2946, 2293, 2253, 1437, 1379, 1119, 1046, 915, 752. HRMS (ESI) m/z: $[M - Cl]^+$ calcd for $C_{54}H_{44}N_3O_2$ 766.3428, found, 766.3455.

(Z)-3-(9-(2-((Hex-5-yn-1-yloxy)carbonyl)phenyl)-6-(1-methyl-2-phenylindolizin-3-yl)-3H-xanthen-3-ylidene)-1-methyl-2-phenyl-3H-indolizin-4-ium hexafluorophosphate (C4CC-RI). To a flame-dried round-bottom flask were added 3′,6′-bis(1-methyl-2-phenylindolizin-3-yl)-3*H*-spiro[isobenzofuran-1,9′-xanthen]-3-one (compound **1**, 50 mg, 0.07 mmol), dry dichloroethane (2 mL, 0.035 M), and then $POCl_3$ (33 μL, 0.35 mmol) dropwise. This solution was degassed with N_2 for 10 min and then refluxed overnight under a N_2 atmosphere. Then, the volatiles were removed via a rotary evaporator. The mixture was diluted with dry dichloromethane (2 mL), degassed with N_2 for 5 min, and then, 5-hexyn-1-ol (10 μL, 0.08 mmol) was added. The mixture was then stirred at room temperature and monitored via absorption spectroscopy. After the product peak ceased to increase in intensity, the volatiles were evaporated and the crude material was stirred in dichloromethane (∼2 mL) over excess solid KPF_6 (∼50 mg) under a nitrogen atmosphere overnight. The solids and the liquids were then separated, the volatiles were evaporated, and the compound was directly subjected to column chromatography using a cyano-functionalized silica column with 10% acetonitrile/90% dichloromethane as the eluent to give the desired dye as a green solid (59%, 33 mg, 0.04 mmol). ^1H NMR (400 MHz, CD_3CN) δ 8.69 (d, J = 7.2 Hz, 2H), 8.30 (d, J = 7.8 Hz, 2H), 7.90−7.77 (m, 2H), 7.62−7.57 (m, 4H), 7.44−7.33 (m, 8H), 7.26−7.23 (m, 4H), 7.18−7.14 (m, 4H), 6.86 (t, J = 6.9 Hz, 2H), 3.95 (t, J = 6.3 Hz, 2H), 2.21 (s, 6H), 2.05−1.98 (m, 3H), 1.44−1.36 (m, 2H), 1.24−1.17 (m, 2H). $^{13}C\{^1H\}$ NMR (100 MHz, CD_3CN) δ 165.7, 156.9, 143.2, 137.6, 134.8, 134.8, 133.7, 133.2, 131.9, 131.5, 131.0, 130.6, 129.9, 129.3, 129.1, 128.3, 124.9, 124.2, 122.6, 122.5, 118.9, 114.8, 114.6, 113.7, 84.2, 69.7, 65.8, 27.6, 25.1, 17.9, 8.9. Note: Two aromatic carbon signals in the ^{13}C spectrum may have identical shifts to reported signals due to significant congestion with 25 expected aromatic signals. Several signals indeed appear significantly larger than other signals in the ^{13}C spectrum. Overlap with the CD_3CN signal is also possible. Limited solubility in CD_3Cl or CD_2Cl_2 prohibits collection of a ^{13}C spectrum and solvents such as d6-DMSO and d6-acetone have appreciable decomposition rates presumably due to residual water in these solvents. ^{19}F NMR (376 MHz, CD_3CN) δ −72.96 (d, J = 705 Hz). ^{31}P NMR (162 MHz, CD_3CN) δ −144.63 (septet, J = 705 Hz). FT-IR (neat, cm^{-1}): 3632, 3541, 3167, 3004, 2946, 2294, 2253, 1445, 1379, 1038, 915, 743. HRMS (ESI) m/z: $[M - Cl]^+$ calcd for $C_{56}H_{43}N_2O_3$ 791.3268; found, 791.3274.

*3′,6′-Dibromo-4,7-dimethyl-3H-spiro[isobenzofuran-1,9′-xanthen]-3-one (compound **5**).* 3,6-Dimethylphthalic anhydride[36] was added to a flame-dried pressure flask (1.00 g, 5.67 mmol). Then, 3-bromophenol (1.2 mL, 11.35 mmol) was added followed by dropwise addition of triflic acid (500 μL, 5.67 mmol). The reaction mixture was sealed and then heated at 140 °C for 72 h. After cooling, the mixture was diluted with ethyl acetate and washed with $NaHCO_3$ (sat. aq.) and brine solutions. The organic layer was then collected, dried over Na_2SO_4, and concentrated under reduced vacuum. The crude mixture was then subjected to silica column chromatography (EtOAc/Hexane) to give a yellow solid (28%, 750 mg, 1.63 mmol). ^1H NMR (400 MHz, $CDCl_3$) δ 7.47 (s, 2H), 7.32−7.27 (m, 1H), 7.18 (d, J = 8.5 Hz, 2H), 6.71 (d, J = 8.5 Hz, 2H), 2.78 (s, 3H), 1.65 (s, 3H). $^{13}C\{^1H\}$ NMR (100 MHz, $CDCl_3$) δ 169.4, 151.3, 150.1, 137.0, 136.7, 132.5, 130.9, 129.0, 127.5, 124.1, 123.4, 120.2, 117.2, 79.6, 17.2, 17.0. FT-IR (neat, cm^{-1}): 3549, 3159, 3004, 2954, 2285, 2254, 1437, 1372, 1046, 906, 743. HRMS (ESI) m/z: $[M + H]^+$ calcd for $C_{22}H_{15}Br_2O_3$ 484.9388; found 484.9360.

*4,7-Dimethyl-3′,6′-bis(1-methyl-2-phenylindolizin-3-yl)-3H-spiro[isobenzofuran-1,9′-xanthen]-3-one (compound **7**).* To a flame-dried pressure flask were added 3′,6′-dibromo-4,7-dimethyl-3H-spiro[isobenzofuran-1,9′-xanthen]-3-one (compound **5**, 500 mg, 1.02 mmol), 1-methyl-2-phenylindolizine (compound **6**, 853 mg, 2.05 mmol), $PdCl_2(PPh_3)_2$ (58 mg, 0.08 mmol), and KOAc (404 mg, 4.1 mmol) inside a nitrogen-filled glovebox. The reaction was removed from the glovebox, and N_2-degassed *N*-methyl-2-pyrrolidone (5 mL, 0.2 M) was added with reaction kept under an inert atmosphere of N_2. The reaction mixture was then heated at 120 °C for 36 h. The mixture was diluted with diethyl ether, washed with water, and dried over Na_2SO_4. The organic layer was then concentrated under reduced pressure and subjected to silica column chromatography with 4% ethyl acetate/96% hexanes as the eluent to get the desired product as a yellow solid (48%, 390 mg, 0.53 mmol). ^1H NMR (400 MHz, CD_2Cl_2) δ 8.02 (d, J = 7.2 Hz, 2H), 7.32 (d, J = 9.0 Hz, 2H), 7.27−7.08 (m, 14H), 6.89−6.85 (m, 2H), 6.73 (d, J = 8.1 Hz, 2H), 6.62 (t, J = 6.4 Hz, 2H), 6.38 (t, J = 6.8 Hz, 2H), 2.66 (s, 3H), 2.24 (s, 6H), 1.62 (s, 3H). ^{13}C NMR (100 MHz, CD_2Cl_2) δ 169.6, 151.4, 136.5, 135.2, 134.4, 132.0, 131.0, 130.8, 130.6, 128.5, 128.0, 126.3, 125.9, 123.5, 121.9, 119.9, 118.1, 117.5, 116.5, 110.7, 107.4, 80.2, 16.9, 16.6, 9.0. Note: Four aromatic carbon signals in the ^{13}C spectrum may have identical shifts to reported signals due to significant congestion with 25 expected aromatic signals. Several signals indeed appear significantly larger than other signals in the ^{13}C spectrum. FT-IR (neat, cm^{-1}): 3059, 2990, 2941, 2292, 2253, 1422, 1374, 1267, 1036, 918, 897, 732, 702. HRMS (ESI) m/z: $[M + H]^+$ calcd for $C_{52}H_{39}N_2O_3$ 739.2961, found 739.2971.

(Z)-3-(9-(2-(Ethoxycarbonyl)-3,6-dimethylphenyl)-6-(1-methyl-2-phenylindolizin-3-yl)-3H-xanthen-3-ylidene)-1-methyl-2-phenyl-3H-indolizin-4-ium hexafluorophosphate (Me2-RI). To a flame-dried round-bottom flask were added 4,7-dimethyl-3′,6′-bis(1-methyl-2-phenylindolizin-3-yl)-3H-spiro[isobenzofuran-1,9′-xanthen]-3-one (compound **7**, 50 mg, 0.06 mmol), dry dichloroethane (2.0 mL, 0.035 M), and $POCl_3$ (32 μL, 0.34 mmol) dropwise. The solution was then degassed with N_2 for 10 min and then refluxed overnight under a N_2 atmosphere. The volatiles were evaporated via a rotary evaporator. Then, the reaction mixture was dissolved in dry dichloromethane, degassed with N_2 for 5 min, and dry ethanol (5 μL, 0.1 mmol) was added. The mixture was then stirred at room temperature and monitored via absorption spectroscopy. After the product peak ceased to increase in intensity, the volatiles were evaporated and the crude material was stirred in dichloromethane (∼2 mL) over excess solid KPF_6 (∼50 mg) under a nitrogen atmosphere overnight. The solids and the liquids were then separated, the volatiles were evaporated, and the compound was directly subjected to column chromatography with a cyano-functionalized silica gel column with 10% acetonitrile/90% dichloromethane as the eluent to give the desired dye as a green solid (59%, 33 mg, 0.04 mmol). ^1H NMR (400 MHz, CD_3CN) δ 8.72 (d, J = 7.1 Hz, 2H), 7.64 (d, J = 9.0 Hz, 2H), 7.57 (s, 2H), 7.49 (s, 2H), 7.44−7.41 (m, 7H), 7.30−7.26 (m, 5H), 7.21−7.17 (m, 4H), 6.90 (t, J = 8.2 Hz, 2H), 3.83 (q, J = 7.1 Hz, 2H), 2.81 (s, 3H), 2.44 (s, 3H), 2.24 (s, 6H), 0.68 (t, J = 7.1 Hz, 3H). $^{13}C\{^1H\}$ NMR (100 MHz, CD_3CN) δ 157.1, 143.5, 137.9, 135.5, 134.9, 134.8, 134.7, 133.4, 133.1, 131.0, 130.1, 129.9, 129.3, 129.2, 128.3, 125.1, 124.4, 122.9, 122.6, 119.0, 114.9, 113.8, 61.7, 19.7, 19.3, 13.4, 8.9. Note: Three aromatic carbon signals in the ^{13}C spectrum may have identical shifts to reported signals due to significant congestion with 25 expected aromatic signals. Several signals indeed appear significantly larger than other signals in the ^{13}C spectrum. Overlap with the CD_3CN signal is also possible. Limited solubility in CD_3Cl or CD_2Cl_2 prohibits collection of a ^{13}C spectrum and solvents such as d6-DMSO and d6-acetone have appreciable decomposition rates presumably due to residual water in these solvents. ^{19}F NMR (376 MHz, CD_3CN) δ −72.96 (d, J = 705 Hz). ^{31}P NMR (162 MHz, CD_3CN) δ −144.63

https://doi.org/10.1021/acs.joc.2c00678
J. Org. Chem. 2022, 87, 11319−11328

(septet, J = 705 Hz). FT-IR (neat, cm^{-1}): 3541, 3167, 3004, 2938, 2302, 2253, 1437, 1030, 915, 743. HRMS (ESI) m/z: [M − Cl]$^+$ calcd for $C_{54}H_{43}N_2O_3$ 767.3268, found, 767.3304.

*3′,6′-Bis(7-(4-(dimethylamino)phenyl)-1-(2-ethylhexyl)-2-phenylindolizin-3-yl)-3H-spiro[isobenzofuran-1,9′-xanthen]-3-one (compound **10**).* To a flame-dried pressure flask were added 3′,6′-dibromo-3*H*-spiro[isobenzofuran-1,9′-xanthen]-3-one (compound **8**, 250 mg, 0.54 mmol), 4-(1-(2-ethylhexyl)-2-phenylindolizin-7-yl)-*N*,*N*-dimethylaniline (compound **9**, 356 mg, 1.09 mmol), $PdCl_2(PPh_3)_2$ (31 mg, 0.04 mmol), and KOAc (161 mg, 1.64 mmol) inside a nitrogen-filled glovebox. The reaction was removed from the glovebox, and N_2 degassed *N*-methyl-2-pyrrolidone (5.0 mL, 0.2 M) was added. The reaction mixture was then heated at 120 °C for 36 h. Next, the reaction mixture was diluted with dichloromethane, washed with water, and dried over Na_2SO_4. The organic layer was then concentrated under reduced pressure and subjected to column chromatography with silica gel and 20% ethyl acetate/80% hexanes as the eluent to give the desired product as a yellow solid (49%, 310 mg, 0.27 mmol). ^{1}H NMR (400 MHz, CD_2Cl_2) δ 8.10 (d, J = 7.5 Hz, 2H), 7.91 (d, J = 7.6 Hz, 1H), 7.65−7.61 (m, 1H), 7.56 (m, 1H), 7.50−7.42 (m, 6H), 7.28−7.10 (m, 13H), 6.89−6.86 (m, 2H), 6.75−6.62 (m, 8H), 2.90 (s, 12H), 2.69−2.56 (m, 4H), 1.33−1.21 (m, 2H), 1.18−0.97 (m, 16H), 0.70 (t, J = 6.7 Hz, 6H), 0.62 (t, J = 7.3 Hz, 6H). ^{13}C NMR (100 MHz, CD_2Cl_2) δ 169.0, 152.6, 151.4, 150.0, 135.8, 135.2, 134.6, 131.9, 130.8, 130.0, 129.5, 128.0, 127.1, 126.5, 126.4, 125.5, 125.0, 124.1, 122.1, 119.6, 117.8, 116.9, 112.9, 112.7, 112.4, 110.0, 82.4, 40.9, 40.3, 32.6, 28.7, 28.1, 25.8, 23.0, 13.9, 10.7. Note: Three aromatic carbon signals in the ^{13}C spectrum may have identical shifts to reported signals due to significant congestion with 25 expected aromatic signals. Several signals indeed appear significantly larger than other signals in the ^{13}C spectrum. FT-IR (neat, cm^{-1}): 3164, 3059, 2941, 2362, 2291, 2252, 1626, 1438, 1421, 1374, 1269, 1036, 918, 733, 702. HRMS (ESI) m/z: [M + H]$^+$ calcd for $C_{80}H_{81}N_4O_3$ 1145.6309, found, 1145.6350.

(Z)-7-(4-(Dimethylamino)phenyl)-3-(6-(7-(4-(dimethylamino)-phenyl)-1-(2-ethylhexyl)-2-phenylindolizin-3-yl)-9-(2-(ethoxycarbonyl)phenyl)-3H-xanthen-3-ylidene)-1-(2-ethylhexyl)-2-phenyl-3H-indolizin-4-ium hexafluorophosphate (7-DMA-RI). To a flame-dried round-bottom flask were added 3′,6′-bis(7-(4-(dimethylamino)phenyl)-1-(2-ethylhexyl)-2-phenylindolizin-3-yl)-3H-spiro[isobenzofuran-1,9′-xanthen]-3-one (compound **10**, 50 mg, 0.06 mmol), dry dichloroethane (2.0 mL, 0.035 M), and $POCl_3$ (20 μL, 0.2 mmol) dropwise. The solution was degassed with N_2 for 10 min and then refluxed overnight under a N_2 atmosphere. The volatiles were evaporated via a rotary evaporator. Then, the reaction mixture was dissolved in dry dichloromethane, degassed with N_2 for 5 min, and dry ethanol (5 μL, 0.1 mmol) was added. The mixture was then stirred at room temperature and monitored via absorption spectroscopy. After the product peak ceased to increase in intensity, the volatiles were evaporated and the crude material was stirred in dichloromethane (∼2 mL) over excess solid KPF_6 (∼50 mg) under a nitrogen atmosphere overnight. The solids and the liquids were then separated, the volatiles were evaporated, and the compound was directly subjected to column chromatography with a cyano-functionalized silica gel column with 5% acetonitrile/95% dichloromethane as the eluent to give the desired dye as a green solid (59%, 33 mg, 0.04 mmol). ^{1}H NMR (400 MHz, CD_3CN) δ 8.51 (d, J = 7.3 Hz, 2H), 8.28−8.20 (m, 1H), 7.82−7.71 (m, 2H), 7.61 (d, J = 9.0 Hz, 6H), 7.40−7.30 (m, 6H), 7.20−7.06 (m, 11H), 6.94 (d, J = 9.0 Hz, 2H), 6.78 (d, J = 8.8 Hz, 4H), 3.98 (q, J = 7.1 Hz, 2H), 2.98 (br s, 12H), 2.57 (br s, 4H), 1.30−1.25 (m, 2H), 1.13−1.03 (m, 16H), 0.95 (t, J = 7.1 Hz, 3H), 0.73 (t, J = 7.1 Hz, 6H), 0.62 (t, J = 7.2 Hz, 6H). ^{13}C{^{1}H} NMR (100 MHz, CD_3CN) δ 165.7, 157.1, 156.0, 151.6, 140.7, 139.5, 137.2, 136.3, 135.2, 133.6, 131.8, 131.4, 130.9, 129.3, 128.3, 127.7, 125.6, 124.7, 123.2, 122.3, 120.7, 113.0, 112.7, 112.1, 62.1, 40.7, 40.0, 32.8, 28.8, 28.2, 26.1, 23.2, 13.9, 13.7, 10.7. Note: Two aromatic carbon signals in the ^{13}C spectrum may have identical shifts to reported signals due to significant congestion with 25 expected aromatic signals. Several signals indeed appear significantly larger than other signals in the ^{13}C spectrum. Overlap with the CD_3CN signal is also possible. Limited solubility in CD_3Cl or CD_2Cl_2 prohibits collection of a ^{13}C spectrum and solvents such as d6-DMSO and d6-acetone have appreciable decomposition rates presumably due to residual water in these solvents. ^{19}F NMR (376 MHz, CD_3CN) δ −72.96 (d, J = 705 Hz). ^{31}P NMR (162 MHz, CD_3CN) δ −144.63 (septet, J = 705 Hz). FT-IR (neat, cm^{-1}): 3555, 3539, 3164, 3004, 2944, 2628, 2362, 2340, 2292, 2252, 1632, 1441, 1418, 1375, 1038, 917, 748. HRMS (ESI) m/z: [M − Cl]$^+$ calcd for $C_{82}H_{85}N_4O_3$ 1173.6616, found, 1173.6643.

Nanoencapsulation. A chloroform solution of 3 mM Triton X100 and a second chloroform solution of 10 mM RI were mixed in a ratio of 10:1 (Triton X100 solution/RI solution). Then, the chloroform was fully evaporated via a rotary evaporator, and the green residue was dissolved in 10 mL of deionized water with stirring and sonication. The solution was syringe-filtered (0.45 μm, nylon) to remove any unloaded dye, and DLS was performed to determine the size of the particles. The nanoparticle solution shows an average particle size of 136 nm.

Relative Quantum Yields. The emission data was collected in toluene or in water at 25 μM dye concentration with a Horiba PTI QuantaMaster QM-8075-21 fluorimeter using an InGaAs detector. The detector was cooled with liquid nitrogen for 2 h prior to recording emission data. C4CC-RI, AMD-RI, and Me2-RI were excited at 919 nm and 7-DMA-RI was excited at 992 nm. The quantum yield (Φ) values were obtained using IR-1061 with a reference quantum yield value of 0.32 ± 0.04% as reported by Sletten and co-workers (Table 1).[39] Quantum yield values taking IR-1061 to have a quantum yield of 0.59% are reported in Table S1.[40] The integrated fluorescence intensity values (estimated using Origin software after base-line correction) and their absorbance at the excitation wavelength were used to calculate the values using the equation below[44]

$$\frac{\Phi_f^s}{\Phi_f^R} = \frac{n_s^2}{n_R^2} \times \frac{\int_0^\infty I_f^s(\lambda_{Ex}, \lambda_{Em})d\lambda_{Em}}{\int_0^\infty I_f^R(\lambda_{Ex}, \lambda_{Em})d\lambda_{Em}} \times \frac{(1 - 10^{-A^R(\lambda_{Ex})})}{(1 - 10^{-A^S(\lambda_{Ex})})}$$

where "Φ" denotes the quantum yield, "I" refers to the integrated fluorescence intensity, "A" is the absorbance at the excitation wavelength, "n" is the refractive index, "s" is the sample, and "R" is the reference standard chosen for the quantum yield studies.

Computational Approach. All of the molecules were first drawn in ChemDraw (20.0.0.41) and saved as MDL Molfile. The geometries of those molecules were then optimized with the MMFF94 force field using Avogado (1.2.0). Dihedral angles of acyclic single bonds were manually set between 0 and 90° to avoid local minima conformations. Then, sequential geometry optimizations were performed by DFT using Gaussian 16[35] with the B3LYP[33,34] functional and the following basis sets: first 3-21G, then 6-31G(d,p),[45,46] and finally, 6-311G-(d,p)[32] with a dichloromethane polarizable continuum model.[29−31] After having the optimized geometries, TD-DFT was performed with the B3LYP functional and 6-311G(d,p) basis set to compute the vertical transition energies and oscillator strengths.

Crystallography Information. Crystallization was performed using a vapor diffusion method. Specifically, an inner open topped 4 mL vial with 10 mg of ^{Ph}RosIndz dissolved in 1 mL of 1,2-dichlorobenzene was placed in a larger 20 mL vial containing 4 mL of diethyl ether. The larger vial was sealed and kept in the dark. Crystal growth was observed within 2 days as a result of the slow diffusion of diethyl ether inside the sample chamber. The 0.17 × 0.05 × 0.03 mm crystal was mounted on a Rigaku XtaLAB Synergy, Dualflex, HyPix diffractometer, and data collection was performed at 299 K. The structure was solved using the Olex2,[47] ShelXT[48] program using the intrinsic phasing method and refined with ShelXL[49] least square package.

■ ASSOCIATED CONTENT

Supporting Information

The Supporting Information is available free of charge at https://pubs.acs.org/doi/10.1021/acs.joc.2c00678.

https://doi.org/10.1021/acs.joc.2c00678
J. Org. Chem. 2022, 87, 11319−11328

NMR spectra, dynamic light scattering data, quantum yield data, computational data, and crystallographic data (PDF)

Accession Codes

CCDC 2157064 contains the supplementary crystallographic data for this paper. These data can be obtained free of charge via www.ccdc.cam.ac.uk/data_request/cif, or by emailing data_request@ccdc.cam.ac.uk, or by contacting The Cambridge Crystallographic Data Centre, 12 Union Road, Cambridge CB2 1EZ, UK; fax: +44 1223 336033.

AUTHOR INFORMATION

Corresponding Authors

Nathan I. Hammer − *Department of Chemistry and Biochemistry, University of Mississippi, University, Mississippi 38677, United States;* orcid.org/0000-0002-6221-2709; Email: nhammer@olemiss.edu

Jared H. Delcamp − *Department of Chemistry and Biochemistry, University of Mississippi, University, Mississippi 38677, United States;* orcid.org/0000-0001-5313-4078; Email: delcamp@olemiss.edu

Authors

Satadru Chatterjee − *Department of Chemistry and Biochemistry, University of Mississippi, University, Mississippi 38677, United States*

Abdul Kalam Shaik − *Department of Chemistry and Biochemistry, University of Mississippi, University, Mississippi 38677, United States;* orcid.org/0000-0001-9704-9254

Kalpani Hirunika Wijesinghe − *Department of Chemistry and Biochemistry, University of Mississippi, University, Mississippi 38677, United States;* orcid.org/0000-0002-7049-0370

David Ndaleh − *Department of Chemistry and Biochemistry, University of Mississippi, University, Mississippi 38677, United States;* orcid.org/0000-0001-6705-6197

Amala Dass − *Department of Chemistry and Biochemistry, University of Mississippi, University, Mississippi 38677, United States;* orcid.org/0000-0001-6942-5451

Complete contact information is available at: https://pubs.acs.org/10.1021/acs.joc.2c00678

Notes

The authors declare the following competing financial interest(s): Several of the authors are on a patent related to the dyes in this manuscript. This is noted in the manuscript.

ACKNOWLEDGMENTS

Authors S.C., A.K.S., D.N., N.I.H., and J.H.D. thank the National Science Foundation for supporting this work through NSF award 1757220. K.H.W. and A.D. thank National Science Foundation grant CHE-1808138.

REFERENCES

(1) Liu, D.; He, Z.; Zhao, Y.; Yang, Y.; Shi, W.; Li, X.; Ma, H. Xanthene-Based NIR-II Dyes for in Vivo Dynamic Imaging of Blood Circulation. *J. Am. Chem. Soc.* **2021**, *143*, 17136−17143.

(2) Liu, M. H.; Zhang, Z.; Yang, Y. C.; Chan, Y. H. Polymethine-Based Semiconducting Polymer Dots with Narrow-Band Emission and Absorption/Emission Maxima at NIR-II for Bioimaging. *Angew. Chem., Int. Ed.* **2021**, *60*, 983−989.

(3) Sun, C.; Li, B.; Zhao, M.; Wang, S.; Lei, Z.; Lu, L.; Zhang, H.; Feng, L.; Dou, C.; Yin, D.; Xu, H.; Cheng, Y.; Zhang, F. J-Aggregates of Cyanine Dye for NIR-II in Vivo Dynamic Vascular Imaging Beyond 1500 nm. *J. Am. Chem. Soc.* **2019**, *141*, 19221−19225.

(4) Wang, S.; Fan, Y.; Li, D.; Sun, C.; Lei, Z.; Lu, L.; Wang, T.; Zhang, F. Anti-Quenching NIR-II Molecular Fluorophores for in Vivo High-Contrast Imaging and pH Sensing. *Nat. Commun.* **2019**, *10*, No. 1058.

(5) Li, Y.; Liu, Y.; Li, Q.; Zeng, X.; Tian, T.; Zhou, W.; Cui, Y.; Wang, X.; Cheng, X.; Ding, Q.; Wang, X.; Wu, J.; Deng, H.; Li, Y.; Meng, X.; Deng, Z.; Hong, X.; Xiao, Y. Novel NIR-II Organic Fluorophores for Bioimaging Beyond 1550 nm. *Chem. Sci.* **2020**, *11*, 2621−2626.

(6) Lu, L.; Li, B.; Ding, S.; Fan, Y.; Wang, S.; Sun, C.; Zhao, M.; Zhao, C. X.; Zhang, F. NIR-II Bioluminescence for in Vivo High Contrast Imaging and in Situ ATP-Mediated Metastases Tracing. *Nat. Commun.* **2020**, *11*, No. 4192.

(7) Cosco, E. D.; Arus, B. A.; Spearman, A. L.; Atallah, T. L.; Lim, I.; Leland, O. S.; Caram, J. R.; Bischof, T. S.; Bruns, O. T.; Sletten, E. M. Bright Chromenylium Polymethine Dyes Enable Fast, Four-Color in Vivo Imaging with Shortwave Infrared Detection. *J. Am. Chem. Soc.* **2021**, *143*, 6836−6846.

(8) Ding, F.; Zhan, Y.; Lu, X.; Sun, Y. Recent Advances in near-Infrared II Fluorophores for Multifunctional Biomedical Imaging. *Chem. Sci.* **2018**, *9*, 4370−4380.

(9) Carr, J. A.; Aellen, M.; Franke, D.; So, P. T. C.; Bruns, O. T.; Bawendi, M. G. Absorption by Water Increases Fluorescence Image Contrast of Biological Tissue in the Shortwave Infrared. *Proc. Natl. Acad. Sci. U.S.A.* **2018**, *115*, 9080−9085.

(10) Rüttger, F.; Mindt, S.; Golz, C.; Alcarazo, M.; John, M. Isomerization and Dimerization of Indocyanine Green and a Related Heptamethine Dye. *Eur. J. Org. Chem.* **2019**, *2019*, 4791−4796.

(11) Chatterjee, S.; Meador, W. E.; Smith, C.; Chandrasiri, I.; Zia, M. F.; Nguyen, J.; Dorris, A.; Flynt, A.; Watkins, D. L.; Hammer, N. I.; Delcamp, J. H. SWIR Emissive Rosindolizine Dyes with Nanoencapsulation in Water Soluble Dendrimers. *RSC Adv.* **2021**, *11*, 27832−27836.

(12) Sreejith, S.; Divya, K. P.; Ajayaghosh, A. A near-Infrared Squaraine Dye as a Latent Ratiometric Fluorophore for the Detection of Aminothiol Content in Blood Plasma. *Angew. Chem., Int. Ed.* **2008**, *47*, 7883−7887.

(13) Ajayaghosh, A. Chemistry of Squaraine-Derived Materials: Near-Ir Dyes, Low Band Gap Systems, and Cation Sensors. *Acc. Chem. Res.* **2005**, *38*, 449−459.

(14) Anees, P.; Sreejith, S.; Ajayaghosh, A. Self-Assembled near-Infrared Dye Nanoparticles as a Selective Protein Sensor by Activation of a Dormant Fluorophore. *J. Am. Chem. Soc.* **2014**, *136*, 13233−13239.

(15) Beija, M.; Afonso, C. A.; Martinho, J. M. Synthesis and Applications of Rhodamine Derivatives as Fluorescent Probes. *Chem. Soc. Rev.* **2009**, *38*, 2410−2433.

(16) Zhao, J.; Zhong, D.; Zhou, S. NIR-I-to-NIR-II Fluorescent Nanomaterials for Biomedical Imaging and Cancer Therapy. *J. Mater. Chem. B* **2018**, *6*, 349−365.

(17) Antaris, A. L.; Chen, H.; Cheng, K.; Sun, Y.; Hong, G.; Qu, C.; Diao, S.; Deng, Z.; Hu, X.; Zhang, B.; Zhang, X.; Yaghi, O. K.; Alamparambil, Z. R.; Hong, X.; Cheng, Z.; Dai, H. A Small-Molecule Dye for NIR-II Imaging. *Nat. Mater.* **2016**, *15*, 235−242.

(18) Smith, A. M.; Mancini, M. C.; Nie, S. Bioimaging: Second Window for in Vivo Imaging. *Nat. Nanotechnol.* **2009**, *4*, 710−711.

(19) Grimm, J. B.; Klein, T.; Kopek, B. G.; Shtengel, G.; Hess, H. F.; Sauer, M.; Lavis, L. D. Synthesis of a Far-Red Photoactivatable Silicon-Containing Rhodamine for Super-Resolution Microscopy. *Angew. Chem., Int. Ed.* **2016**, *55*, 1723−1727.

(20) Sun, Y. Q.; Liu, J.; Lv, X.; Liu, Y.; Zhao, Y.; Guo, W. Rhodamine-Inspired Far-Red to near-Infrared Dyes and Their Application as Fluorescence Probes. *Angew. Chem., Int. Ed.* **2012**, *51*, 7634−7636.

(21) Davies, K. S.; Linder, M. K.; Kryman, M. W.; Detty, M. R. Extended Rhodamine Photosensitizers for Photodynamic Therapy of Cancer Cells. *Bioorg. Med. Chem.* **2016**, *24*, 3908−3917.
(22) Ando, N.; Soutome, H.; Yamaguchi, S. Near-Infrared Fluorescein Dyes Containing a Tricoordinate Boron Atom. *Chem. Sci.* **2019**, *10*, 7816−7821.
(23) Koide, Y.; Kojima, R.; Hanaoka, K.; Numasawa, K.; Komatsu, T.; Nagano, T.; Kobayashi, H.; Urano, Y. Design Strategy for Germanium-Rhodamine Based pH-Activatable near-Infrared Fluorescence Probes Suitable for Biological Applications. *Commun. Chem.* **2019**, *2*, No. 94.
(24) Grimm, J. B.; Muthusamy, A. K.; Liang, Y.; Brown, T. A.; Lemon, W. C.; Patel, R.; Lu, R.; Macklin, J. J.; Keller, P. J.; Ji, N.; Lavis, L. D. A General Method to Fine-Tune Fluorophores for Live-Cell and in Vivo Imaging. *Nat. Methods* **2017**, *14*, 987−994.
(25) Rathnamalala, C. S. L.; Gayton, J. N.; Dorris, A. L.; Autry, S. A.; Meador, W.; Hammer, N. I.; Delcamp, J. H.; Scott, C. N. Donor-Acceptor-Donor NIR II Emissive Rhodindolizine Dye Synthesized by C-H Bond Functionalization. *J. Org. Chem.* **2019**, *84*, 13186−13193.
(26) Rathnamalala, C. S. L.; Pino, N. W.; Herring, B. S.; Hooper, M.; Gwaltney, S. R.; Chan, J.; Scott, C. N. Thienylpiperidine Donor NIR Xanthene-Based Dye for Photoacoustic Imaging. *Org. Lett.* **2021**, *23*, 7640−7644.
(27) Qi, Q.; Chi, W.; Li, Y.; Qiao, Q.; Chen, J.; Miao, L.; Zhang, Y.; Li, J.; Ji, W.; Xu, T.; et al. A H-Bond Strategy to Develop Acid-Resistant Photoswitchable Rhodamine Spirolactams for Super-Resolution Single-Molecule Localization Microscopy. *Chem. Sci.* **2019**, *10*, 4914−4922.
(28) Uno, S.-N.; Kamiya, M.; Yoshihara, T.; Sugawara, K.; Okabe, K.; Tarhan, M. C.; Fujita, H.; Funatsu, T.; Okada, Y.; Tobita, S.; Urano, Y. A Spontaneously Blinking Fluorophore Based on Intramolecular Spirocyclization for Live-Cell Super-Resolution Imaging. *Nat. Chem.* **2014**, *6*, 681−689.
(29) Miertus, S.; Scrocco, E.; Tomasi, J. Electrostatic Interaction of a Solute with a Continuum. A Direct Utilization of Ab Initio Molecular Potentials for the Prevision of Solvent Effects. *Chem. Phys.* **1981**, *55*, 117−129.
(30) Miertus, S.; Tomasi, J. Approximate Evaluations of the Electrostatic Free Energy and Internal Energy Changes in Solution Processes. *Chem. Phys.* **1982**, *65*, 239−245.
(31) Pascual-Ahuir, J. L.; Silla, E.; Tunon, I. Gepol: An Improved Description of Molecular Surfaces. III. A New Algorithm for the Computation of a Solvent-Excluding Surface. *J. Comput. Chem.* **1994**, *15*, 1127−1138.
(32) Frisch, M. J.; Pople, J. A.; Binkley, J. S. Self-Consistent Molecular Orbital Methods 25. Supplementary Functions for Gaussian Basis Sets. *J. Chem. Phys.* **1984**, *80*, 3265−3269.
(33) Becke, A. D. Density-Functional Thermochemistry. III. The Role of Exact Exchange. *J. Chem. Phys.* **1993**, *98*, 5648−5652.
(34) Lee, C.; Yang, W.; Parr, R. G. Development of the Colle-Salvetti Correlation-Energy Formula into a Functional of the Electron Density. *Phys. Rev. B* **1988**, *37*, 785−789.
(35) Frisch, M. J.; Trucks, G. W.; Schlegel, H. B.; Scuseria, G. E.; Robb, M. A.; Cheeseman, J. R.; Scalmani, G.; Barone, V.; Petersson, G. A.; Nakatsuji, H.; Li, X.; Caricato, M.; Marenich, A. V.; Bloino, J.; Janesko, B. G.; Gomperts, R.; Mennucci, B.; Hratchian, H. P.; Ortiz, J. V.; Izmaylov, A. F.; Sonnenberg, J. L.; Williams-Young, D.; Ding, F.; Lipparini, F.; Egidi, F.; Goings, J.; Peng, B.; Petrone, A.; Henderson, T.; Ranasinghe, D.; Zakrzewski, V. G.; Gao, J.; Rega, N.; Zheng, G.; Liang, W.; Hada, M.; Ehara, M.; Toyota, K.; Fukuda, R.; Hasegawa, J.; Ishida, M.; Nakajima, T.; Honda, Y.; Kitao, O.; Nakai, H.; Vreven, T.; Throssell, K.; Montgomery, J. A., Jr.; Peralta, J. E.; Ogliaro, F.; Bearpark, M. J.; Heyd, J. J.; Brothers, E. N.; Kudin, K. N.; Staroverov, V. N.; Keith, T. A.; Kobayashi, R.; Normand, J.; Raghavachari, K.; Rendell, A. P.; Burant, J. C.; Iyengar, S. S.; Tomasi, J.; Cossi, M.; Millam, J. M.; Klene, M.; Adamo, C.; Cammi, R.; Ochterski, J. W.; Martin, R. L.; Morokuma, K.; Farkas, O.; Foresman, J. B.; Fox, D. J. *Gaussian 16*, Revision C.01; Gaussian, Inc.: Wallingford CT, 2016.
(36) Abel, B. A.; Lidston, C. A. L.; Coates, G. W. Mechanism-Inspired Design of Bifunctional Catalysts for the Alternating Ring-Opening Copolymerization of Epoxides and Cyclic Anhydrides. *J. Am. Chem. Soc.* **2019**, *141*, 12760−12769.
(37) Woodroofe, C. C.; Lim, M. H.; Bu, W.; Lippard, S. J. Synthesis of Isomerically Pure Carboxylate- and Sulfonate-Substituted Xanthene Fluorophores. *Tetrahedron* **2005**, *61*, 3097−3105.
(38) Ndaleh, D.; Smith, C.; Loku Yaddehige, M.; Shaik, A. K.; Watkins, D. L.; Hammer, N. I.; Delcamp, J. H. Shortwave Infrared Absorptive and Emissive Pentamethine-Bridged Indolizine Cyanine Dyes. *J. Org. Chem.* **2021**, *86*, 15376−15386.
(39) Cosco, E. D.; Caram, J. R.; Bruns, O. T.; Franke, D.; Day, R. A.; Farr, E. P.; Bawendi, M. G.; Sletten, E. M. Flavylium Polymethine Fluorophores for near- and Shortwave Infrared Imaging. *Angew. Chem., Int. Ed.* **2017**, *56*, 13126−13129.
(40) Hoshi, R.; Suzuki, K.; Hasebe, N.; Yoshihara, T.; Tobita, S. Absolute Quantum Yield Measurements of near-Infrared Emission with Correction for Solvent Absorption. *Anal. Chem.* **2020**, *92*, 607−611.
(41) Semonin, O. E.; Johnson, J. C.; Luther, J. M.; Midgett, A. G.; Nozik, A. J.; Beard, M. C. Absolute Photoluminescence Quantum Yields of IR-26 Dye, PbS, and PbSe Quantum Dots. *J. Phys. Chem. Lett.* **2010**, *1*, 2445−2450.
(42) Friedman, H. C.; Cosco, E. D.; Atallah, T. L.; Jia, S.; Sletten, E. M.; Caram, J. R. Establishing Design Principles for Emissive Organic SWIR Chromophores from Energy Gap Laws. *Chem* **2021**, *7*, 3359−3376.
(43) Ansteatt, S.; Meares, A.; Ptaszek, M. Amphiphilic near-IR-Emitting 3,5-Bis(2-Pyrrolylethenyl)Bodipy Derivatives: Synthesis, Characterization, and Comparison with Other (Hetero)Arylethenyl-Substituted Bodipys. *J. Org. Chem.* **2021**, *86*, 8755−8765.
(44) Levitus, M. Tutorial: Measurement of Fluorescence Spectra and Determination of Relative Fluorescence Quantum Yields of Transparent Samples. *Methods Appl. Fluoresc.* **2020**, *8*, No. 033001.
(45) Hehre, W. J.; Ditchfield, R.; Pople, J. A. Self—Consistent Molecular Orbital Methods. XII. Further Extensions of Gaussian—Type Basis Sets for Use in Molecular Orbital Studies of Organic Molecules. *J. Chem. Phys.* **1972**, *56*, 2257−2261.
(46) Francl, M. M.; Pietro, W. J.; Hehre, W. J.; Binkley, J. S.; Gordon, M. S.; DeFrees, D. J.; Pople, J. A. Self-Consistent Molecular Orbital Methods. XXIII. A Polarization-Type Basis Set for Second-Row Elements. *J. Chem. Phys.* **1982**, *77*, 3654−3665.
(47) Dolomanov, O. V.; Bourhis, L. J.; Gildea, R. J.; Howard, J. A. K.; Puschmann, H. Olex2: A Complete Structure Solution, Refinement and Analysis Program. *J. Appl. Crystallogr.* **2009**, *42*, 339−341.
(48) Sheldrick, G. M. Shelxt - Integrated Space-Group and Crystal-Structure Determination. *Acta Crystallogr., Sect. A: Found. Adv.* **2015**, *71*, 3−8.
(49) Sheldrick, G. M. Crystal Structure Refinement with Shelxl. *Acta Crystallogr., Sect. C: Struct. Chem.* **2015**, *71*, 3−8.

https://doi.org/10.1021/acs.joc.2c00678
J. Org. Chem. 2022, 87, 11319−11328